



Coordination-Driven Self-Assembly of Silver(I) and Gold(I) Rings: Synthesis, Characterization, and Photophysical Studies

Cressa Ria P. Fulong¹, Sewon Kim¹, Alan E. Friedman² and Timothy R. Cook^{1*}

¹ Department of Chemistry, University at Buffalo, The State University of New York, Buffalo, NY, United States, ² Department of Materials Design and Innovation, University at Buffalo, The State University of New York, Buffalo, NY, United States

OPEN ACCESS

Edited by:

Luís D. Carlos,
University of Aveiro, Portugal

Reviewed by:

Fernando Novio,
Catalan Institute of Nanoscience and
Nanotechnology (GIN2), Spain
Lin Xu,
East China Normal University, China

*Correspondence:

Timothy R. Cook
trcook@buffalo.edu

Specialty section:

This article was submitted to
Inorganic Chemistry,
a section of the journal
Frontiers in Chemistry

Received: 28 February 2019

Accepted: 26 July 2019

Published: 13 August 2019

Citation:

Fulong CRP, Kim S, Friedman AE and
Cook TR (2019) Coordination-Driven
Self-Assembly of Silver(I) and Gold(I)
Rings: Synthesis, Characterization,
and Photophysical Studies.
Front. Chem. 7:567.
doi: 10.3389/fchem.2019.00567

In this work, we investigate the self-assembly between Ag(I) and Au(I) centers and pyridyl donors to form hexagonal metallacycles and related linear complexes. The precipitation of hexagonal metallacycles upon assembly in chloroform/methanol mixtures results in high solid-state photo-stability. Whereas, the Ag(I) species have fast kinetics and high formation constants in acetone, this solvent interferes in the formation of the analogous Au(I) complexes. The photophysical properties of this suite of metallacycles was investigated including steady-state absorption, emission, and time-resolved lifetime measurements. All ligands and hexagons exhibited ligand-centered singlet emissions with ground-state absorption and emission perturbed upon coordination. The ligand-based fluorescent photoluminescence was affected by the heavy-atom effect when halide or metals are present, attenuating quantum yields as evidenced by increases in the experimentally measured non-radiative rate constants. The formation of group 11 metallacycles is motivated by their potential applications in mixed-matrix materials wherein metal ions can interact with substrate to facilitate separations chemistry with reduced energy requirements, in particular the isolation of ethylene and light olefins. Existing processes involve cryogenic distillation, an energy intensive and inefficient method.

Keywords: self-assembly, coordination, metallacycle, silver hexagon, gold hexagon

INTRODUCTION

Coordination-driven self-assembly (Leininger et al., 2000) is a valuable strategy for the design and synthesis of discrete molecular complexes such as metallacycles and metallacages for biomedical (Cook et al., 2013; Casini et al., 2017) catalytic (Ito et al., 2000; Brown et al., 2009; Smulders and Nitschke, 2012; Vardhan and Verpoort, 2015; Kuijpers et al., 2016), molecular sensing (Tashiro et al., 2005; Kim and Ahn, 2008; Wang et al., 2011; Zwijnenburg et al., 2016; Cao et al., 2017), and small molecule adsorption and separation applications (Sudik et al., 2005; Zhao et al., 2010; Riddell et al., 2011; Amayuelas et al., 2016). This strategy exploits pre-programmed directionality information on metal acceptor and ligand donor building blocks to form complex architectures driven by metal-ligand coordination (Cook and Stang, 2015). A careful design of building blocks coupled with thermodynamic driving forces favors the convergent formation of discrete molecular

complexes over divergent coordination polymers a.k.a. metal-organic frameworks (MOFs) (Fujita et al., 2001).

Inspired by previous reports on hexagonal self-assemblies from *trans*-capped Pt(II) precursors (Yang et al., 2007) and 120° bidentate pyridine-type ligands, which are known for their luminescent properties, and other luminescent Pt(II)-based metallacycles (Huang et al., 2017; Tang et al., 2018), we now report the self-assembly of hexagonal metallacycles from the same class of ligand donors and Ag(I) and Au(I) metal acceptors. There have been few reports on linear Ag(I) (Del Piero et al., 2008) and Au(I) (Fernández et al., 2007) complexes, and Ag(I) metallacycles (Shin et al., 2003; Chen and Mak, 2005; Fromm et al., 2005; Ren et al., 2006; Kim et al., 2009; Wan and Mak, 2011; Kole et al., 2012; Wei et al., 2012; Chevrier et al., 2013) with pyridine-type ligands, but these are the first Ag(I) and Au(I) hexagonal rings. We also synthesized Ag(I) and Au(I) monomeric complexes using analogous monodentate pyridine-type ligands. Having both linear monomeric complexes and hexagonal metallacycles enables the comparison of solid- and solution-state structures, organic solvent solubilities, photophysical properties, as well as light-stabilities. These self-assembled Ag(I) and Au(I) hexagons have limited solubility in organic solvents. Efforts are ongoing to improve the solubilities of these metallacycles including but not limited to pre- and post-assembly ligand modification.

We have an ongoing interest in incorporating these metallacycles and metallacages as filler materials in mixed-matrix materials (MMMs) (Fulong et al., 2018). MMMs are a type of thin-film composite material typically composed of a highly porous inorganic/organic filler and an organic polymer binder. The significance of MMMs in the medical and small molecule purification industries has been steadily increasing in the past decade and contemporary research is largely focused on MOFs as a filler material (Dechnik et al., 2017). We have previously shown the importance of solubilizing the filler material into the polymer solution to fabricate thin, flexible, homogeneous, and highly permeable MMMs (Fulong et al., 2018). Along these lines, we highlighted the advantage and ease of using discrete coordination cages over MOFs as MMMs filler material due to the former's solubility in a range of solvents. For certain separations the filler material introduces sites for intermolecular interactions with substrate, which enables active separation rather than just size-selective sieving. As a result, the design of fillers with unsaturated metals or other binding sites enables the fabrication of MMMs with improved permeability and selectivity. Since a variety of metal centers may be used as nodes in coordination-driven self-assembly, properly matching metal ions to a separation of interest is an important first-principle in the design of new metal-organic materials (Dechnik et al., 2017).

The incorporation of silver salts has been identified as an effective strategy for increasing the selectivity of olefin/paraffin membranes based on the ability of electron-rich olefins to interact with metal ions, an attractive technology given the scope of the petrochemical industry wherein ethylene is used a primary building block (Eldridge, 1993). These materials suffer from the instability of Ag(I) ions that react with oxygen

and leach from the material. We hypothesized that Ag(I) ions may be stabilized by a linear L–Ag(I)–L environment that still enables equatorial interactions with substrate (Fox et al., 2002; Gimeno, 2009). Other transition metals with coordination numbers of three or more require capping ligands to prevent divergent framework formation (Fujita, 1998; Fujita et al., 2001). For Ag(I) and Au(I), with linear coordination environments, capping ligands are not required and coordination with bent ditopic donors may furnish discrete metallacycles.

MATERIALS AND METHODS

All reagents and solvents were reagent grade and used as received without further purification unless noted. Methanol (CH₃OH), acetone, dichloromethane (DCM), ethyl acetate (EtOAc), *n*-hexanes, toluene, diethyl ether, petroleum ether, potassium hydroxide (KOH), sodium sulfate (Na₂SO₄) and potassium carbonate (K₂CO₃) were purchased from Fisher Scientific. *N,N*-dimethylformamide (DMF) was purchased from Macron Fine Chemicals. Tetrahydrofuran (THF), triethylamine (NEt₃), and chloroform (CHCl₃) were purchased from EMD Millipore. Ethanol (EtOH, 200 proof) was purchased from Decon Labs, Inc. Tetrakis(triphenylphosphine)palladium(0) (Pd(PPh₃)₄), and bis(triphenylphosphine)palladium(II) chloride (Pd(PPh₃)₂Cl₂), and 1,3-dibromobenzene were purchased from Matrix Scientific. 4-pyridinylboronic acid (pyB(OH)₂) was purchased from AK Scientific. Copper (I) iodide (CuI) was purchased from Strem Chemicals. Tetrahydrothiophene (tht) was purchased from Aldrich. Silver(I) hexafluorophosphate (AgPF₆) was purchased from Oakwood Chemical. Hydrogen tetrachloroaurate(III) trihydrate (HAuCl₄·3H₂O) was purchased from J&J Materials Inc. 4-ethynylpyridine hydrochloride and 1,3,5-tribromobenzene were purchased from Ark Pharm Inc. Deionized water was used whenever water was needed. THF was purified and dried through a Pure Process Technology free standing solvent purification system. NEt₃ was purified and dried by distillation in KOH. DMF was filtered and dried using activated molecular sieves under N₂ and freeze-pump-thawed with water before use for synthesis.

¹H Nuclear Magnetic Resonance (NMR) spectra were recorded on either Varian 300 or 400 MHz spectrometer. Chemical shifts (δ) are reported in parts per million (ppm) referenced using the residual protio-solvent peaks as internal standards. Coupling constants (J) are quoted in Hertz (Hz), and the following abbreviations are used to describe the signal multiplicities: s (singlet); d (doublet); t (triplet); q (quartet); m (multiplet). Fourier Transform-Ion Cyclotron Resonance (FT-ICR) mass spectra were acquired using a Bruker Daltonics SolariX 12T FT-ICR Mass Spectrometer that was calibrated with > 90% Angiotensin I purchased from Sigma Aldrich under either Electrospray Ionization (ESI) or Laser Desorption Ionization (LDI) modes. Single Crystal X-ray Diffraction (SC-XRD) Crystallography was performed using a Bruker D8 Venture diffractometer in a fixed-chi geometry, equipped with a Photon-100 CMOS area detector, Oxford Cryosystems cryostat, a molybdenum

source (Mo, $\lambda = 0.71073 \text{ \AA}$), and a graphite monochromator. Fourier Transform Infrared Resonance (FT-IR) spectra were collected from a Perkin Elmer 1760 FT-IR spectrometer equipped with horizontal attenuated total reflectance (HATR) from 4,000 to 500 cm^{-1} wavenumbers (ν). The following abbreviations are used to describe signal intensities: w (weak); m (medium); s (strong). All UV-Vis absorption spectra were acquired from an Agilent Cary 8454 UV-Vis Diode Array system. Blank spectra with pure solvents were acquired before each run. All emission spectra were collected using a Horiba Scientific FluoroMax-4 Spectrofluorometer equipped with Quanta- ϕ Integrating light sphere with Spectralon coating for quantum yield (Φ) measurements and Delta-Hub DH-HT High Throughput Time-correlated Single Photon Counting (TCSPC) Controller and Nano-LED NL-C2 pulsed-diode controller with N-350 NanoLED Source for lifetime measurements. All solution-state absorbance and emission spectra were collected using a 10-mm rectangular quartz cuvette from Starna Cells Inc.

Synthesis of Ag(I) Complex (AgL₁)

AgL₁ complex was self-assembled using a modified literature procedure (Chen et al., 2013). In a foil-covered 200-mL round-bottom flask, 0.800 g (3.1 mmol) L1 was dissolved in 80.0 mL CHCl₃. In another foil-covered 100-mL round-bottom flask, 0.720 g (2.85 mmol) AgPF₆ was dissolved in 80.0 mL MeOH then layered over the L1 solution. After 48 h, white needle-like crystals form. These crystals were filtered and washed with 10-mL portions of CHCl₃ (3x) to afford 1.19 g (100% yield) isolated product. ¹H NMR (400 MHz, acetone-d₆, 25°C): δ (ppm) = 8.81 (d, ³J = 5.2 Hz, 4H, pyridyl H _{α}), 7.82 (s, 2H, phenyl H), 7.77 (d, ³J = 6.3 Hz, 4H, pyridyl H _{β}), 7.71 (d, ³J = 8.1 Hz, 2H, phenyl H), 7.65 (d, ³J = 7.8 Hz, 2H, phenyl H), 7.46 (t, ³J = 7.9 Hz, 2H, phenyl H). FT-IR (ATR, cm⁻¹): 3069 (w), 2235 (w), 2187 (w), 1609 (m), 1558 (w), 1506 (w), 1470 (w), 1433 (w), 1405 (w), 1223 (w), 1152 (w), 1070 (w), 1031 (w), 991 (w), 915 (w), 881 (m), 815 (m), 775 (m), 757 (m), 743 (m), 678 (m), 663 (m), 553 (m), 531 (m).

Synthesis of ({AgL₂})₆ Ag(I) Hexagon

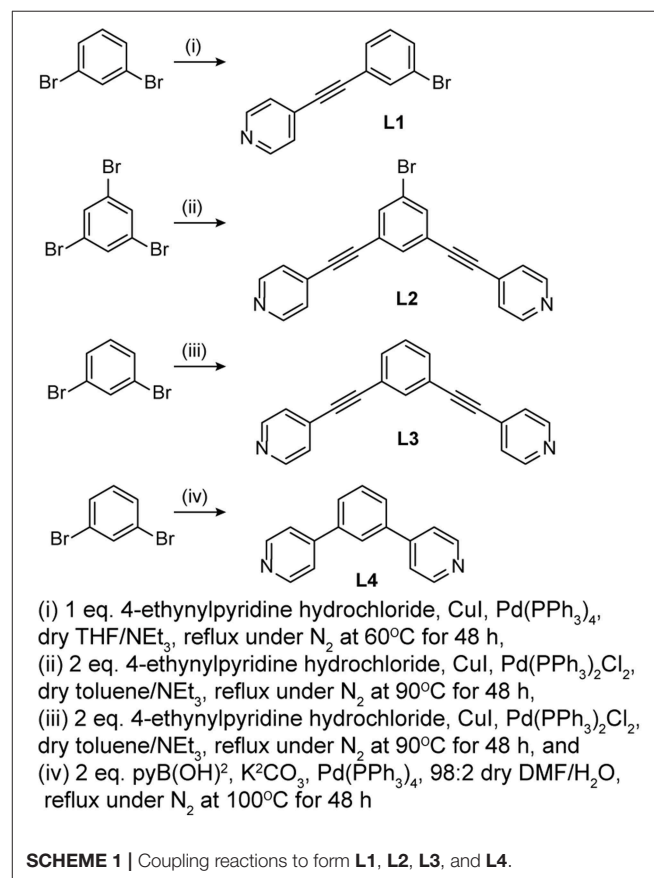
{AgL₂}₆ hexagon, was self-assembled using a modified literature procedure (Chen et al., 2013). In a foil-covered 20-mL scintillation vial, 0.050 g (0.14 mmol) L2 was dissolved in 5.0 mL CHCl₃. In another foil-covered 20-mL scintillation vial, 0.035 g (0.14 mmol) AgPF₆ was dissolved in 5.0 mL MeOH then layered over the L2 solution. After 48 h, white powdered product formed which was filtered and washed with 10-mL portions of CHCl₃ (3x) to afford 0.062 g (73% yield) isolated product. ¹H NMR (400 MHz, acetone-d₆, 25°C): δ (ppm) = 8.72 (d, ³J = 5.9 Hz, 24H, pyridyl H _{α}), 7.90 (s, 11H, phenyl H), 7.83 (s, 6H, phenyl H), 7.62 (d, ³J = 6.0 Hz, 24H, pyridyl H _{β}). FT-IR (ATR, cm⁻¹): 3076 (w), 2219 (w), 1613 (m), 1557 (w), 1507 (w), 1435 (m), 1338 (w), 1291 (w), 1221 (m), 1174 (w), 1162 (w), 1136 (w), 1107 (w), 1066 (w), 1028 (w), 993 (w), 964 (w), 864 (m), 821 (s), 748 (w), 736 (w), 663 (m), 573 (w), 552 (s).

Synthesis of ({AgL₃})₆ Ag(I) Hexagon

{AgL₃}₆ hexagon, was self-assembled using a modified literature procedure (Chen et al., 2013). In a foil-covered 20-mL scintillation vial, 0.050 g (0.18 mmol) L3 was dissolved in 5.0 mL CHCl₃. In another foil-covered 20-mL scintillation vial, 0.045 g (0.18 mmol) AgPF₆ was dissolved in 5.0 mL MeOH then layered over the L3 solution. After 48 h, white powdered product formed which was filtered and washed with 10-mL portions of CHCl₃ (3x) to afford 0.096 g (100% yield) isolated product. ¹H NMR (400 MHz, acetone-d₆, 25°C): δ (ppm) = 8.74 (d, ³J = 6.0 Hz, 24H, pyridyl H _{α}), 7.86 (s, 6H, phenyl H), 7.74 (d, ³J = 9.3 Hz, 12H, phenyl H), 7.66 (d, ³J = 6.1 Hz, 23H, pyridyl H _{β}), 7.63 – 7.56 (m, 7H, phenyl H). FT-IR (ATR, cm⁻¹): 3107 (w), 2203 (w), 1615 (m), 1543 (w), 1501 (w), 1431 (w), 1227 (w), 1167 (w), 1064 (w), 1025 (w), 878 (w), 821 (m), 752 (w), 733 (w), 682 (w), 556 (m), 541 (m).

Synthesis of ({AgL₄})₆ Ag(I) Hexagon

{AgL₄}₆ hexagon, was self-assembled using a modified literature procedure (Chen et al., 2013). In a foil-covered 20-mL scintillation vial, 0.025 g (0.11 mmol) L4 was dissolved in 2.0 mL CHCl₃. In another foil-covered 20-mL scintillation vial, 0.027 g (0.11 mmol) AgPF₆ was dissolved in 2.0 mL MeOH then layered over the L4 solution. After 48 h, white powdered product formed which was filtered and washed with 10-mL portions of CHCl₃



(3x) to afford 0.052 g (92% yield) isolated product. $^1\text{H NMR}$ (400 MHz, acetone- d_6 , 25°C): δ (ppm) = 8.76 (d, $^3J = 6.7$ Hz, 24H, pyridyl H_α), 8.25 (s, 5H, phenyl H), 8.00–7.87 (m, 36H, pyridyl H_β and phenyl H), 7.80–7.71 (m, 5H, phenyl H). FT-IR (ATR, cm^{-1}): 3092 (w), 1618 (m), 1545 (w), 1513 (w), 1478 (w), 1431 (w), 1411 (w), 1314 (w), 1230 (w), 1069 (w), 1031 (w), 1019 (w), 873 (m), 818 (s), 791 (s), 736 (m), 695 (m), 663 (w), 637 (m), 613 (w), 555 (s).

Synthesis of Au(I) Complex (AuL_2)

AuL_2 complex was self-assembled using a modified literature procedure (Lin et al., 2008). In a foil-covered 2-dram vial, 0.020 g (0.078 mmol) **L1**, 0.025 g (0.078 mmol) $\text{Au}(\text{tht})\text{Cl}$ were dissolved in 6.0 mL acetone. After 6 h, the solution was concentrated in vacuo and the collected solid was washed with 6-mL portions of CHCl_3 (3x) to afford 0.007 g (20% yield) isolated product. $^1\text{H NMR}$ (300 MHz, acetone- d_6 , 25°C): δ (ppm) = 8.84 (d, $^3J = 6.0$ Hz, 4H, pyridyl H_α), 7.89 (d, $^3J = 7.0$ Hz, 5H, pyridyl H_β), 7.80 (s, 2H, phenyl H), 7.68 (td, $^3J = 16.3, 15.7, 7.8$ Hz, 10H), 7.50–7.40 (m, 3H, phenyl H). FT-IR (ATR, cm^{-1}): 3044 (w), 2918 (w), 2856 (w), 2218 (m), 2187 (w), 1943 (w), 1801 (w), 1614 (m), 1588 (m), 1558 (w), 1496 (w), 1463 (w), 1429 (w), 1404 (w), 1261 (w), 1234 (w), 1217 (w), 1158 (w), 1105 (w), 1088 (w), 1060 (w), 1038 (w), 987 (w), 906 (w), 876 (w), 836 (m), 814 (w), 789 (m), 747 (w), 713 (w), 691 (w), 680 (m), 655 (m), 565 (w), 535 (m).

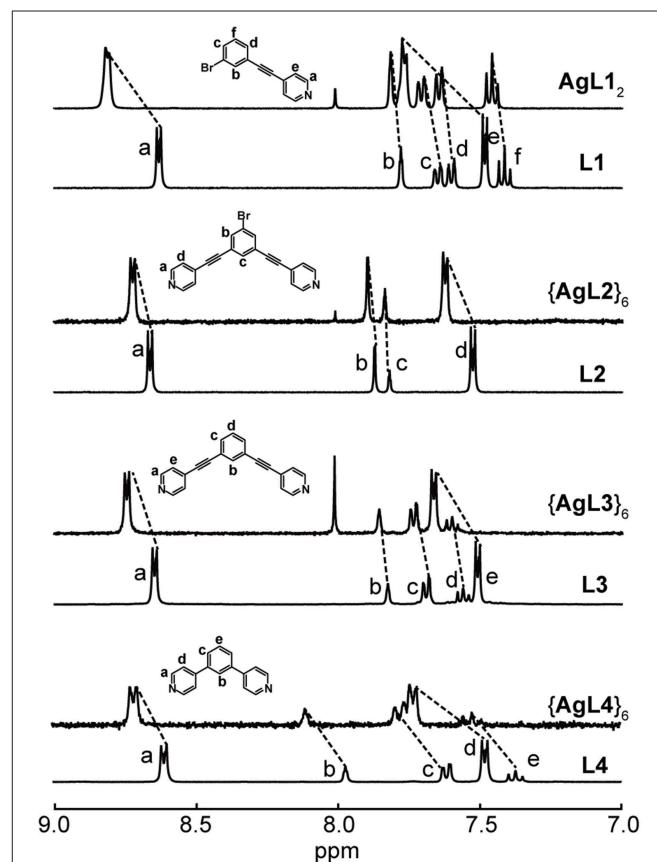
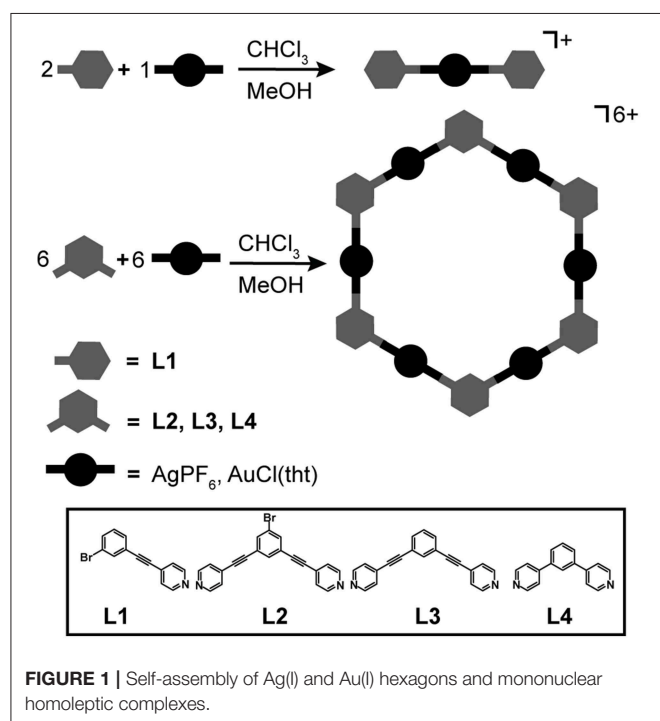
Synthesis of Au(I) Hexagons ($\{\text{AuL}_2\}_6$)

$\{\text{AuL}_2\}_6$ hexagon was self-assembled using a modified literature procedure (Lin et al., 2008). In a foil-covered 2-dram vial, 0.028 g (0.078 mmol) **L2**, 0.025 g (0.078 mmol) $\text{Au}(\text{tht})\text{Cl}$ were dissolved in 6.0 mL CHCl_3 . After 24 h, the solution was concentrated in

vacuo and the collected yellow solid was washed with 6-mL portions of CHCl_3 (3x) to afford 0.025 g (78% yield) isolated product. $^1\text{H NMR}$ (400 MHz, CD_3NO_3 , 25°C): δ (ppm) = 8.84–8.71 (m, 24H, pyridyl H_α), 8.09–7.82 (m, 40H, pyridyl H_β and phenyl H). FT-IR (ATR, cm^{-1}): 3100 (w), 3044 (w), 2210 (m), 1615 (s), 1553 (w), 1496 (w), 1430 (m), 1336 (w), 1288 (w), 1211 (m), 1171 (w), 1134 (w), 1105 (w), 1063 (m), 1046 (w), 992 (w), 966 (w), 863 (m), 826 (m), 761 (w), 721 (w), 672 (m), 587 (w), 574 (m), 527 (w).

Synthesis of Au(I) Hexagons ($\{\text{AuL}_3\}_6$)

$\{\text{AuL}_3\}_6$ hexagon was self-assembled using a modified literature procedure (Lin et al., 2008). In a foil-covered 2-dram vial, 0.022 g (0.078 mmol) **L3**, 0.025 g (0.078 mmol) $\text{Au}(\text{tht})\text{Cl}$ were dissolved in 6.0 mL CHCl_3 . After 24 h, the solution was concentrated in vacuo and the collected yellow solid was washed with 6-mL portions of CHCl_3 (3x) to afford 0.026 g (89% yield) isolated product. $^1\text{H NMR}$ (400 MHz, CD_3NO_3 , 25°C): δ (ppm) = 8.76 (d, $^3J = 5.0$ Hz, 24H, pyridyl H_α), 8.08–7.70 (m, 41H, pyridyl H_β and phenyl H), 7.66–7.57 (m, 7H, phenyl H). FT-IR (ATR, cm^{-1}): 3092 (w), 3029 (w), 2203 (m), 1943 (w), 1609 (s), 1529 (w), 1492 (w), 1427 (w), 1324 (w), 1213 (w), 1162 (w), 1150 (w), 1125 (w), 1093 (w), 1065 (w), 1042 (w), 991 (w), 942 (w), 902 (w), 831 (m), 792 (w), 754 (w), 729 (w), 666 (w), 569 (w), 544 (w).



Synthesis of Au(I) Hexagons ($\{AuL_4\}_6$)

$\{AuL_4\}_6$ hexagon was self-assembled using a modified literature procedure (Lin et al., 2008). In a foil-covered 2-dram vial, 0.018 g (0.078 mmol) **L4**, 0.025 g (0.078 mmol) Au(tht)Cl were dissolved in 6.0 mL $CHCl_3$. After 24 h, the solution was concentrated in vacuo and the collected white solid was washed with 6-mL portions of $CHCl_3$ (3x) to afford 0.027 g (100% yield) isolated product. 1H NMR (400 MHz, CD_3NO_3 , 25°C): δ (ppm) = 8.82 (d, $^3J = 6.7$ Hz, 24H, pyridyl H_α), 8.35 (s, 7H, phenyl H), 8.22 (d, $^3J = 6.3$ Hz, 22H, pyridyl H_β), 8.11 (d, $^3J = 9.4$ Hz, 14H, phenyl H), 7.86 (t, $^3J = 7.6$ Hz, 7H, phenyl H). FT-IR (ATR, cm^{-1}): 3060 (w), 1611 (s), 1546 (w), 1508 (w), 1472 (w), 1443 (w), 1427 (w), 1398 (m), 1340 (w), 1318 (w), 1266 (w), 1231 (m), 1186 (w), 1109 (w), 1076 (m), 1034 (w), 970 (w), 935 (w), 915 (w), 857 (w), 832 (m), 786 (s), 761 (w), 732 (m), 687 (w), 667 (w), 645 (m), 632 (w), 606 (w), 535 (s).

RESULTS AND DISCUSSION

Self-Assembly of Ag(I) and Au(I) Complexes and Hexagons

Four pyridyl ligands, 1-bromo-3(4-ethynylpyridyl)benzene (**L1**), 5-bromo-1,3-bis(4-ethynylpyridyl)benzene (**L2**), 1,3-bis(4-ethynylpyridyl)benzene (**L3**), and 1,3-bis(4-pyridyl)benzene (**L4**), were prepared as donors for self-assembly reactions. As illustrated in **Scheme 1**, **L1**, **L2**, and **L3** were prepared following a typical Sonogashira coupling reaction while **L4** was prepared following a typical Suzuki coupling reaction. The 1H NMR spectra of **L1**, **L2**, **L3**, and **L4** in acetone- d_6 are summarized in **Supplementary Figures 1A–D**, respectively. The **L1** 1H spectrum shows the pyridyl-H doublets at 8.63 and 7.49 ppm and the benzyl-H singlet at 7.78 ppm, two doublets at 7.65 and 7.60 ppm, and triplet at 7.42 ppm. The **L2** spectrum shows the pyridyl-H doublets at 8.66 and 7.53 ppm and the benzyl-H singlets at 7.87 and 7.82 ppm. The **L3** spectrum shows the pyridyl-H doublets at 8.65 and 7.51 ppm and the benzyl-H singlet at 7.83 ppm, doublet at 7.69 ppm, and triplet at 7.56 ppm. The **L4** spectrum shows the pyridyl-H doublets at 8.68 and 7.78 ppm and the benzyl-H singlet at 8.17 ppm, doublet at 7.89 ppm, and triplet at 7.70 ppm.

L1 was used to synthesize linear Ag(I) and Au(I) complexes, while **L2**, **L3**, and **L4** were used to self-assemble Ag(I) and Au(I) hexagonal metallacycles. The general method used to self-assemble the complexes and hexagons is shown in **Figure 1**. All self-assembly reactions were performed in the absence of light to ensure no loss in Ag(I) and Au(I) precursors. The monomeric Ag(I) complex, AgL_1_2 , was prepared by layering one equivalent of $AgPF_6$ in MeOH over two equivalents of **L1** in $CHCl_3$. This resulted in the crystallization of AgL_1_2 after 48 h. Ag(I) hexagons, $\{AgL\}_6$ where **L** = **L2**, **L3**, and **L4**, were prepared by layering one equivalent of $AgPF_6$ in MeOH over one equivalent of **L** in $CHCl_3$. The hexagons precipitated at almost quantitative yields as white powders after 48 h. The gold analogs, Au(I) hexagons, $\{AuL\}_6$ where **L** = **L2**, **L3**, and **L4**, were prepared by mixing 1:1 equivalents of Au(tht)Cl and **L** in $CHCl_3$. After 24 h, powdered metallacycles were isolated upon solvent removal and $CHCl_3$

washing. In the case of the monomeric Au(I) complex, AuL_1_2 , previous attempts using pure $CHCl_3$ or 1:1 (v/v) $CHCl_3/MeOH$ did not result in any complex formation. However, the complex was isolated at a relatively low yield by mixing 1:1 equivalents of Au(tht)Cl and **L1** in acetone.

1H NMR of Ag(I) and Au(I) Complexes and Hexagons

A notable challenge in characterizing these self-assembled Ag(I) and Au(I) complex and hexagons is their limited solubilities. Coordinating solvents such as acetonitrile (MeCN) and *N,N'*-dimethylsulfoxide (DMSO), which are typically used in solution-state structural analyses of Ag(I) and Au(I) complexes proved to be unsuitable for our complexes and hexagons (Laye, 2007; Lin et al., 2008). In all cases, we observed ligand dissociation upon addition of MeCN or DMSO.

Nonetheless, we were able to detect the intact Ag(I) complexes and hexagons (**Figure 2**) as well as Au(I) complex (**Figure 3**) in acetone. The coordination of the pyridyl ligands to Ag(I) and Au(I) is exemplified by the characteristic downfield shifts in 1H NMR peaks as well as peak integration agreements (**Supplementary Figures 2, 3A**). In addition, the same peak splitting patterns between

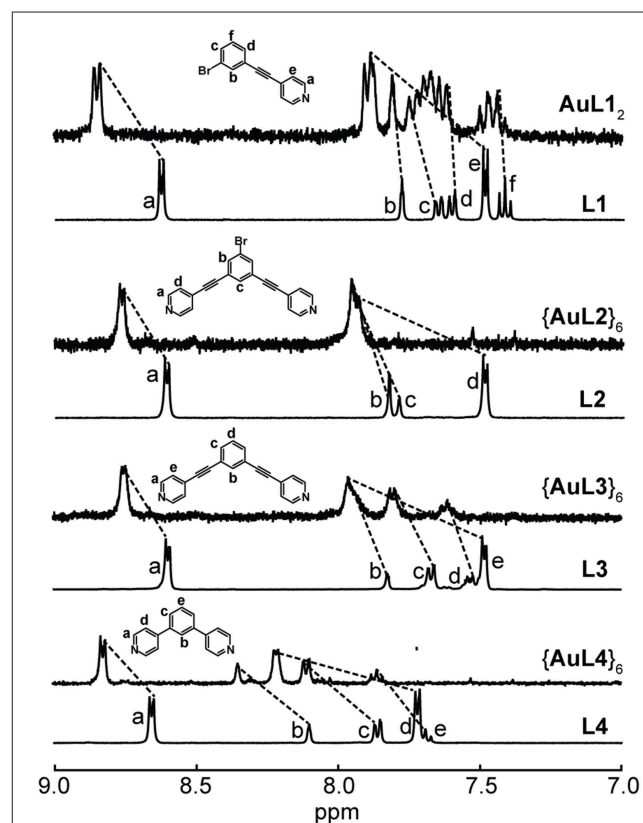


FIGURE 3 | 1H NMR spectra of **L1** and AuL_1_2 in acetone- d_6 , **L2** and $\{AuL_2\}_6$, **L3** and $\{AuL_3\}_6$ and **L4** and $\{AuL_4\}_6$ in nitromethane- d_3 .

the ligand and the complex/hexagon were expected due to the C_{2v} symmetry of both AgL_2 and AuL_2 complexes and the D_{6h} symmetry of all $\{AgL\}_6$ hexagonal metallacycles.

For the Au(I) hexagons, ligand dissociation occurs when MeCN, DMSO, and acetone were used as solvents. These hexagons are insoluble in all other solvents except for nitromethane, in which we were able to observe intact Au(I) hexagons. **Figure 3** summarizes the 1H NMR spectra of $\{AuL_2\}_6$, $\{AuL_3\}_6$, and $\{AuL_4\}_6$. The full spectra of each Au(I) hexagon are shown in **Supplementary Figures 3B–D**. Similar to the Ag(I) hexagons, the downfield shifts of all 1H NMR peaks, the peak integration agreements, and the similarity in peak splitting patterns indicate the formation of pure Au(I) hexagonal metallacycles. Although the solubility of these species is limited, our identification of NMR-suitable solvents rules out the formation of polymeric species as such coordination polymers

are fully insoluble. ESI-MS (see below) further confirms the stoichiometries of self-assembly.

Formation of Ag(I) and Au(I) Complexes and Hexagons in Acetone

All of these complexes were synthesized in pure $CHCl_3$ or in $CHCl_3$ mixtures with MeOH. MeCN and DMSO competitively coordinate with the Ag(I) and Au(I) resulting in ligand dissociation. Acetone was a suitable solvent for the building blocks, as well as the final assemblies, enabling the study of complex formation. Using 1H NMR methods, we initially acquired a series of spectra for a solution containing 1:1 equivalents of Ag:L in acetone upon mixing and after 24 h (**Supplementary Figure 4**). We observed that the thermodynamic products formed immediately upon mixing with no significant changes observed after 24 h. This suggests a fast

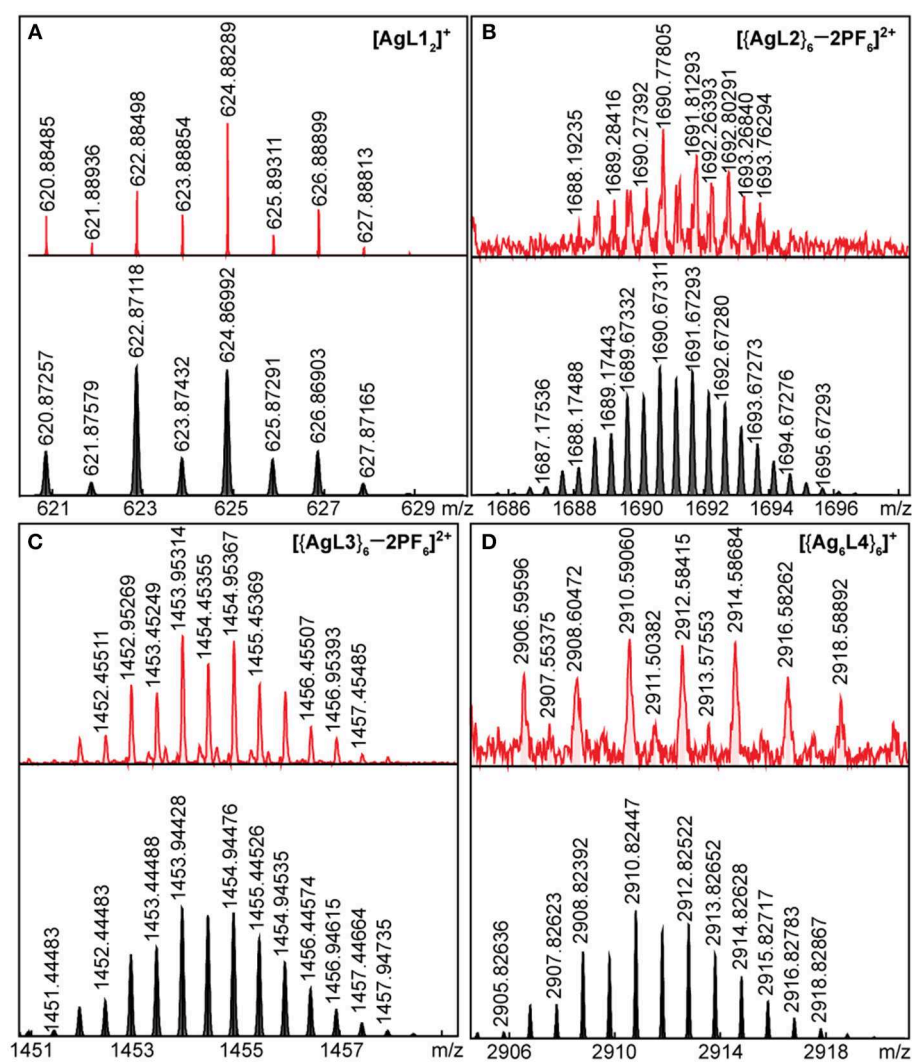


FIGURE 4 | ESI-FT-ICR MS spectrograms of intact (A) AgL_2 , (B) $[AgL_2]_6$, (C) $[AgL_3]_6$, and (D) LDI-FT-ICR MS spectrum of intact $[AgL_4]_6$ (top = experimental, bottom = simulated).

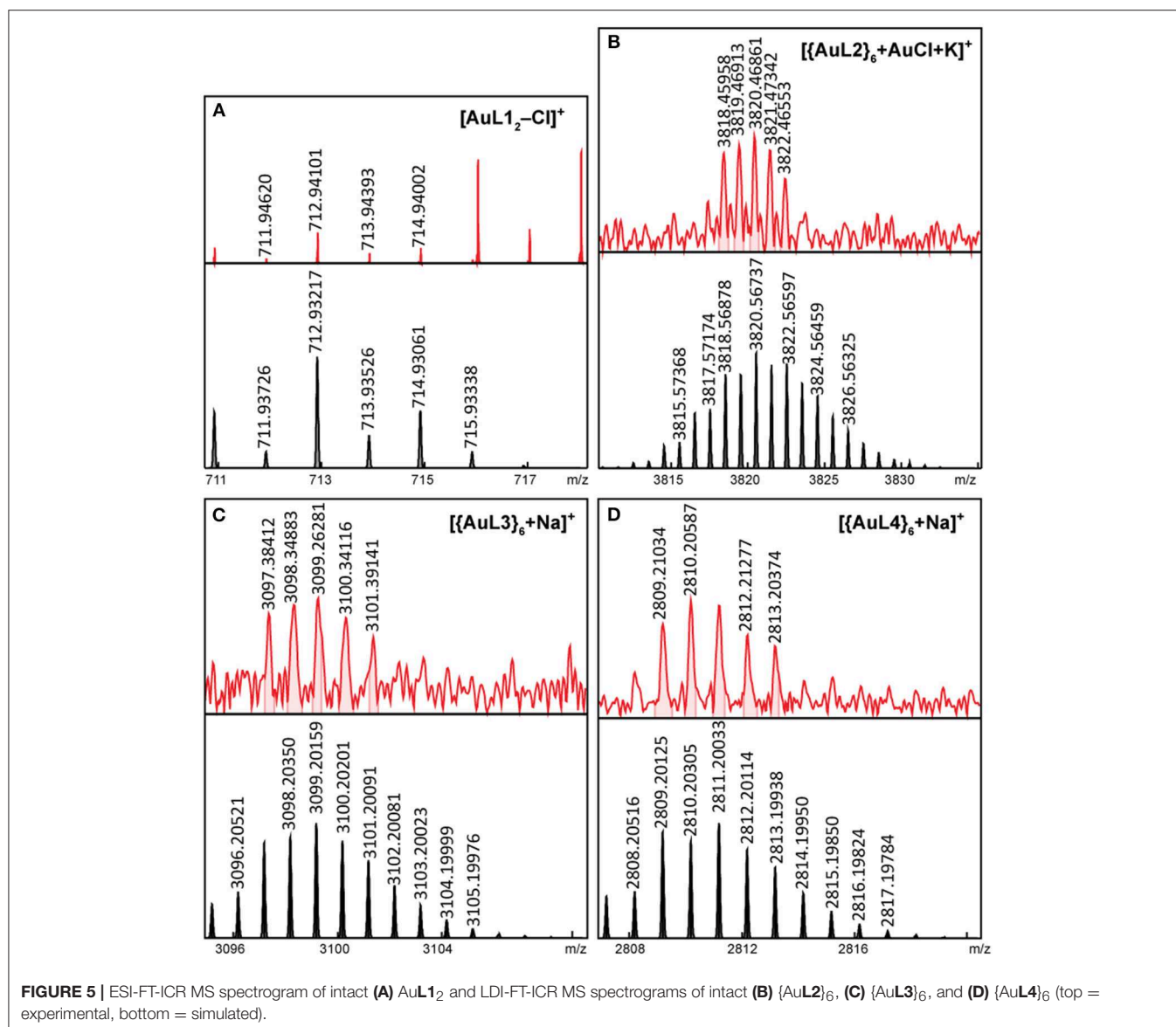
kinetics with a large formation constant for all Ag(I) complex and hexagons in acetone.

Similarly, we wanted to study the solution formation of the Au(I) complex and hexagons. In this case, we prepared solutions containing 1:1, 2:1, and 3:1 equivalents of Au:L in acetone to ensure complete ligand coordination. The acquired ^1H NMR spectra at 0 (upon mixing), 6, 24, and 48 h were summarized in **Supplementary Figures 5–7** for 1:1, 2:1, and 3:1 solutions, respectively. It was observed that the AuL_2 complex self-assembles within 6 h then partially dissociates thereafter. In the case of both $\{\text{AuL}_2\}_6$ and $\{\text{AuL}_3\}_6$, an equilibrium was established immediately upon mixing that stays up to at least 48 h. Products of $\{\text{AuL}_4\}_6$ hexagon assembly crash out of solution immediately upon mixing such that we only observe uncoordinated **L4** and partially dissolved products. In all cases, the initial coordination is fast; however, quantitative analyses of

the NMR peaks is not straightforward using a one-step metal-ligand binding model. There are reports on the mechanism and reducing ability of acetone to form Au nanoparticles from Au(III) and Au(I) (Marin et al., 2008). Thus, we think that there is a possibility of either Au(I) slowly being released as Au(0) from the hexagonal metallacycle into the acetone solution or acetone competitively coordinating to Au(I) to form other products.

FT-ICR MS of Ag(I) and Au(I) Complexes and Hexagons

High-resolution mass spectrometry (HRMS) was used to probe the stoichiometry of our self-assemblies. We used Fourier transform-ion cyclotron mass spectrometry (FT-ICR MS) with electrospray ionization (ESI) for soluble complexes and hexagons, while laser desorption/ionization (LDI) was used for hexagons that are unstable in acetone. ESI, as a soft



ionization technique, is advantageous and popularly used in detection of intact coordination complexes and cages with high molar masses (Vikse and Scott McIndoe, 2018). Typical of soft ionization methods, molecules are ionized by either loss of ions or association with low-valent ions. In the case of our Ag(I) and Au(I) complexes and hexagons, loss of counter-ions results in multiply-charged compounds that are easily detectable by HR-MS at lower m/z . In cases wherein the hexagon is not stable in acetone, we opted to use matrix-free LDI, which uses high-energy lasers to ionize samples in the solid state. LDI is not popularly used in coordination chemistry due to formation of singly-charged fragment ions (Mandal et al., 2019). We, nonetheless, successfully identified intact hexagons in their solid state.

The mass spectrograms for Ag(I) complex and hexagons and for Au(I) complex and hexagons are shown in **Figures 4**, **5**, respectively. For the Ag(I) complex and hexagons, we were able to detect the intact $[\text{AgL}_2]^+$ complex (**Figure 4A**) as well as $[\{\text{AgL}_2\}_6 - 2\text{PF}_6]^{2+}$ hexagon (**Figure 4B**) and $[\{\text{AgL}_3\}_6 - 2\text{PF}_6]^{2+}$ hexagon (**Figure 4C**) by ESI-FT-ICR MS. A loss of one PF_6^- counter-ion was observed for the complex and two PF_6^- were observed for both hexagons. $[\{\text{AgL}_4\}_6]^+$ hexagon (**Figure 4D**), which has low solubility in acetone, was detected by LDI-FT-ICR MS.

For the Au(I) complex and hexagons, we were able to detect the intact $[\text{AuL}_2]^+$ complex (**Figure 5A**) with a loss of Cl^- counter-ion by ESI-FT-ICR MS. The Au(I) hexagons, which are unstable in acetone were detected by LDI-FT-ICR MS. We were able to detect singly-charged intact $[\{\text{AuL}_2\}_6 + \text{AuCl} + \text{K}]^+$ hexagon (**Figure 5B**), $[\{\text{AuL}_3\}_6 + \text{Na}]^+$ hexagon (**Figure 5C**), and $[\{\text{AuL}_4\}_6 + \text{Na}]^+$ hexagon (**Figure 5D**). Each of these hexagons have six chloride counter-ions. We also observed $\{\text{AuL}\}_6$ fragments (**Supplementary Figures 12–15**) with chloride counter-ions by ESI-FT-ICR MS, which further confirms the presence of chloride counter-ions in the Au(I) hexagons.

In all cases, we were able to confirm the presence of intact complexes and cages from the agreement of molecular ion m/z and isotopic distribution pattern between the simulated and experimental spectrograms. The presence of complex and hexagon fragmentation (**Supplementary Figures 8–11** for Ag(I) and **Supplementary Figures 12–15** for Au(I) complexes and hexagons) in the mass spectra further confirmed the structure and counter-ions of the linear complex and hexagonal self-assemblies since these fragments were not detected in the NMR studies.

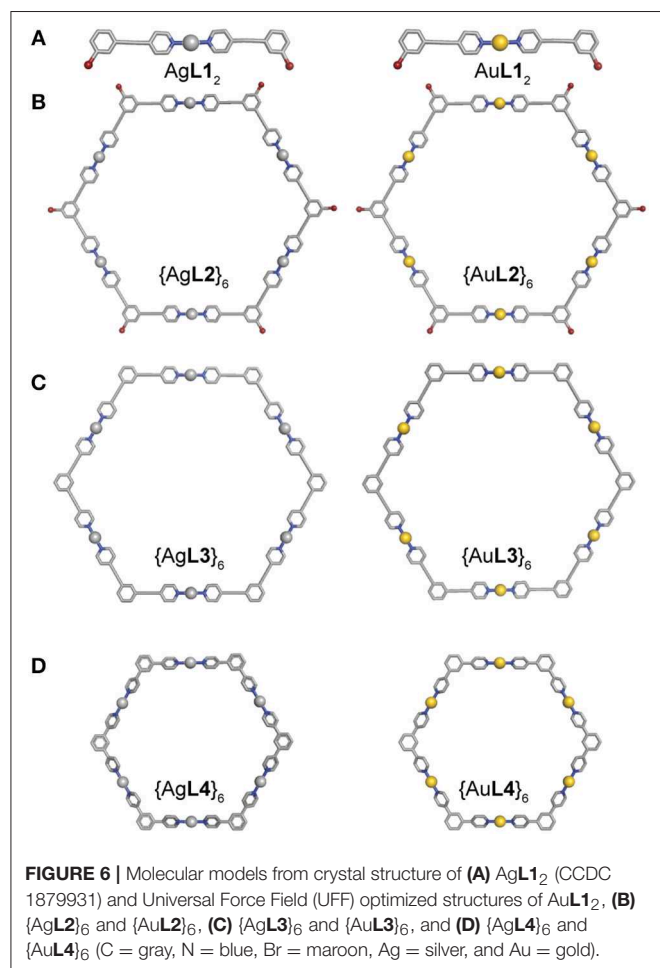
Structures of Ag(I) and Au(I) Complexes and Hexagons

Single-crystal X-ray diffraction was attempted to further elucidate the structures of the Ag(I) and Au(I) complexes and hexagons. Slow evaporation of acetone solutions resulted in very fine needle-like crystals. Only crystals of AgL_2 gave a tractable data set. The asymmetric unit contains two formula units ($Z' = 2$) held in a cofacial conformation as well as a single chloroform molecule. Each Ag(I) center possess a coordination number of 2 with near ideal 180° geometries (**Figure 6A** and **Supplementary Figure 16** and **Table S1**). The PF_6^- counter ion is outer sphere with a closest contact of approximately 3 Å. It is apparent that non-covalent interactions are a strong driving force in the resulting crystal structure of this compound. An apparent argentophilic Ag(I)—Ag(I) interaction leads to the interesting cofacial conformation (~ 3.5 Å). Furthermore, interaction between the electron-rich Br atoms and the H atoms (average separation 3.60(9) Å) of the corresponding formula unit further contribute to the observed structure.

Molecular mechanics geometry optimizations were carried out on the Au(I) complex and the Ag(I) and Au(I) hexagons (**Figures 6B–D**). These structures were optimized using Universal Force Field (UFF) as implemented in ArgusLab. All hexagons formed from **L2** and **L3** preserved ligand planarity. In contrast, the hexagons from **L4** have pyridyl groups that are rotated by 40° from the central phenyl due to the steric strain of the protons on neighboring aromatic rings.

Solid-State Light Stability of Ag(I) and Au(I) Complexes and Hexagons

Solid-state IR spectroscopy is another useful tool to confirm the coordination of the pyridyl ligands to Ag(I) and Au(I) metal acceptors and study the solid-state photostability of the complexes and hexagons. We acquired FT-IR spectra of the



ligands, complexes and hexagons as synthesized. After a week of storing the complexes and hexagons under room light at ambient conditions, we re-acquired the FT-IR spectra of each compound. The ligand IR spectra are shown in both **Figures 7, 8**, where the characteristic aromatic -CH stretching at $3,000\text{--}3,100\text{ cm}^{-1}$, aromatic -CC- stretching at $1,400\text{--}1,600\text{ cm}^{-1}$, and aromatic -CN- stretching at $1,600\text{ cm}^{-1}$ are present in all ligands (Katritzky and Hands, 1958; Schrader, 2007). The characteristic alkyne -CC- stretching at $2,100\text{ cm}^{-1}$ are also present in **L1**, **L2**, and **L3**.

In all cases, there is a slight shift to higher wavenumbers upon Ag(I) or Au(I) coordination, most notably for the -CN- stretching peaks at $1,600\text{ cm}^{-1}$. We observe no change in both the functional group and the fingerprint regions after exposure of the complexes and hexagons to room light for one week, which confirms the improved photo-stability of Ag(I) and Au(I) upon coordination into both linear complex and hexagonal metallacycle.

Photophysical Properties of Ag(I) and Au(I) Complexes and Hexagons

The photophysical properties of these self-assembled complexes and hexagons were studied using steady-state and time-resolved methods. Studies of Ag(I) (Zhou et al., 2006; Laye, 2007; Yeşilil et al., 2012; Mei et al., 2015a; Jenkins and Assefa, 2017) and Au(I) (Lin et al., 2008; Langdon-Jones and Pope, 2014; Shakirova et al., 2017) complexes and metallacycles with N-donor heterocyclic ligands demonstrate interesting luminescent properties, which

assigned to metal-to-ligand charge transfers (MLCT), ligand-based charge transfers, or metal-perturbed ligand-based charge transfers in part due to argentophilic or aurophilic interactions.

We studied both the solution- and solid-state photoluminescence of all Ag(I) and Au(I) complexes and hexagons; however, the acetone instability of some compounds limited our solution-state studies to the photoluminescence of Ag(I) complexes and hexagons and the mononuclear Au(I) complex in acetone. The solution-state absorption and emission of the free ligands, Ag(I) and Au(I) complexes, and Ag(I) hexagons are summarized in **Figure 9**. Several UV-vis absorption features were masked by the UV-cutoff of acetone. Nonetheless, the high energy band due to $\pi \rightarrow \pi^*$ ligand-centered transitions that is typical of aromatic and alkynyl-containing ligands (Shakirova et al., 2017) were prominent in **L1**, **L2**, and **L3** and less so in **L4** due to the absence of ethynyl spacer in this ligand. We see a slight red-shift in the absorption of **AgL1₂** (**Figure 9A**) but not in **AuL1₂** (**Figure 9E**) or any of the Ag(I) hexagons (**Figures 9B–D**) suggesting ligand-centered transitions for the Au(I) complex and Ag(I) hexagons and metal-perturbed ligand-centered transition for the Ag(I) complex, which is supported by the presence of argentophilic interactions in the crystal structure (**Figure 6**).

Table 1 shows the summary of all measured quantum yields (Φ , **Supplementary Figures 17–22**) and lifetimes (τ , **Supplementary Figures 23–25**) and all calculated radiative (k_r) and non-radiative (k_{nr}) decay rate constants. At 330 nm

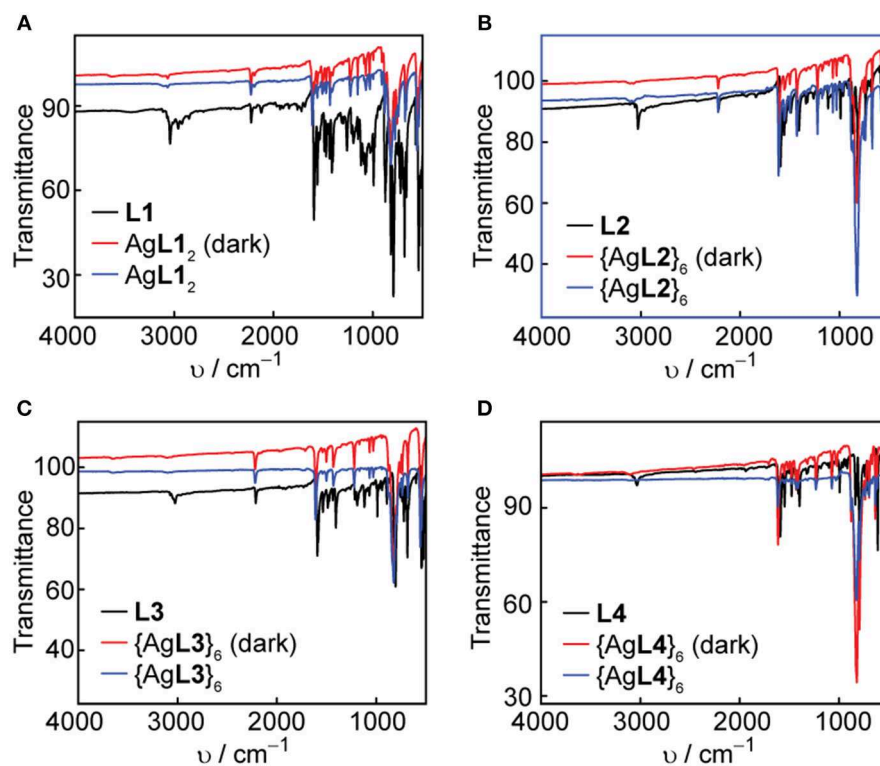


FIGURE 7 | Comparison of FT-IR spectra in the dark and under room light conditions for **(A)** **L1** and **AgL1₂**, **(B)** **L2** and **{AgL2}₆**, **(C)** **L3** and **{AgL3}₆**, and **(D)** **L4** and **{AgL4}₆**.

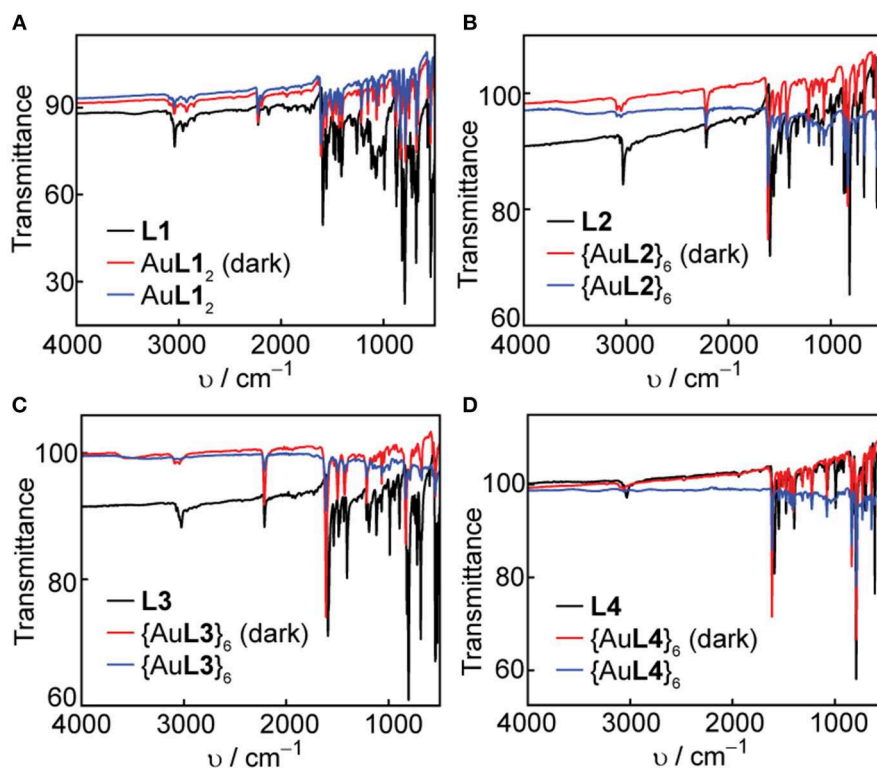


FIGURE 8 | Comparison of FT-IR spectra in the dark and under room light conditions for (A) L1 and AuL1₂, (B) L2 and {AuL2}₆, (C) L3 and {AuL3}₆, and (D) L4 and {AuL4}₆.

excitation, fluorescence emission bands centered at 375 nm (Figures 9A–C) were observed for L1, L2, and L3 in acetone at 3.82, 0.800, and 7.76% quantum yields and 0.11, 0.12, 0.49 ns lifetimes, respectively (Table 1). These ligands have ethynyl spacers that connect the central phenyl group to the pyridyl group/s, which helps rigidify the structure and enhance emission. The highest quantum yield and longest lifetime was observed in L3, which is not affected by heavy-atom effects, unlike L1 and L2 wherein bromide was present. In addition, the four-fold increase in k_{nr} for L1 ($8.91 \times 10^9 \text{ s}^{-1}$) and L2 ($8.00 \times 10^9 \text{ s}^{-1}$) as compared to L3 ($1.89 \times 10^9 \text{ s}^{-1}$), further supports the enhancement of inter-system crossing (ISC) for the bromine-containing ligands. On the other hand, a weak fluorescence band centered at 400 nm (Figure 9D) was observed for L4 but has a quantum yield and lifetime below the limit of our instrumental detection. By placing an upper bound on quantum yield and lifetime of L4 based on instrumental detection limits, we estimated an upper limit to k_r and a lower limit to k_{nr} as shown in Table 1. The absence of the ethynyl spacer in L4 introduces rotational freedom that enhances internal conversion resulting in very weak emission of the ligand.

Similar to the absorption profiles, we also observe a red-shift in the emission band of AgL1₂ centered at 400 nm (Figure 9A) but not in AuL1₂ (375 nm, Figure 9E) or any of the Ag(I) hexagons, {AgL2}₆ (375 nm, Figure 9B), {AgL3}₆ (375 nm, Figure 9C), and {AgL4}₆ (400 nm, Figure 9D). These

emission profiles are similar to that of the ligand with significant reduction in quantum yields and lifetimes upon ligand coordination to Ag(I) and Au(I) suggesting ligand-centered singlet emissions with some perturbations from Ag(I) argentophilic interactions for the Ag(I) complex. Although not as common, fluorescent transition metal complexes are known (Chia and Tay, 2014). The lack of triplet emissions in these complexes can be attributed to either lack of metal-ligand interaction resulting in small metal contribution at the excited state or larger rate constant for fluorescence compared to that of ISC, which is reasonable given the fluorescence emission of the free ligand. Based on our decay rate constant calculations for the Ag(I) and Au(I) complexes and Ag(I) hexagons, k_{nr} is always higher than k_r which implies poor metal-ligand interaction as the main reason for lack of phosphorescence in these compounds.

We also reported the solid-state quantum yields of all ligands, Ag(I) and Au(I) complexes, and hexagons in Table 1. Similar to the solution-state quantum yields, the highest and lowest quantum yields are observed for L3 and L4, respectively. Upon ligand coordination to either Ag(I) and Au(I), we see a general decrease in quantum yields except for {AgL2}₆, {AgL4}₆, and {AgL4}₆. These quantum yield enhancement may be due to aggregation induced emission (Fan et al., 2015; Mei et al., 2015b), particularly in metallacycles containing L4, which in itself is weakly emissive, wherein

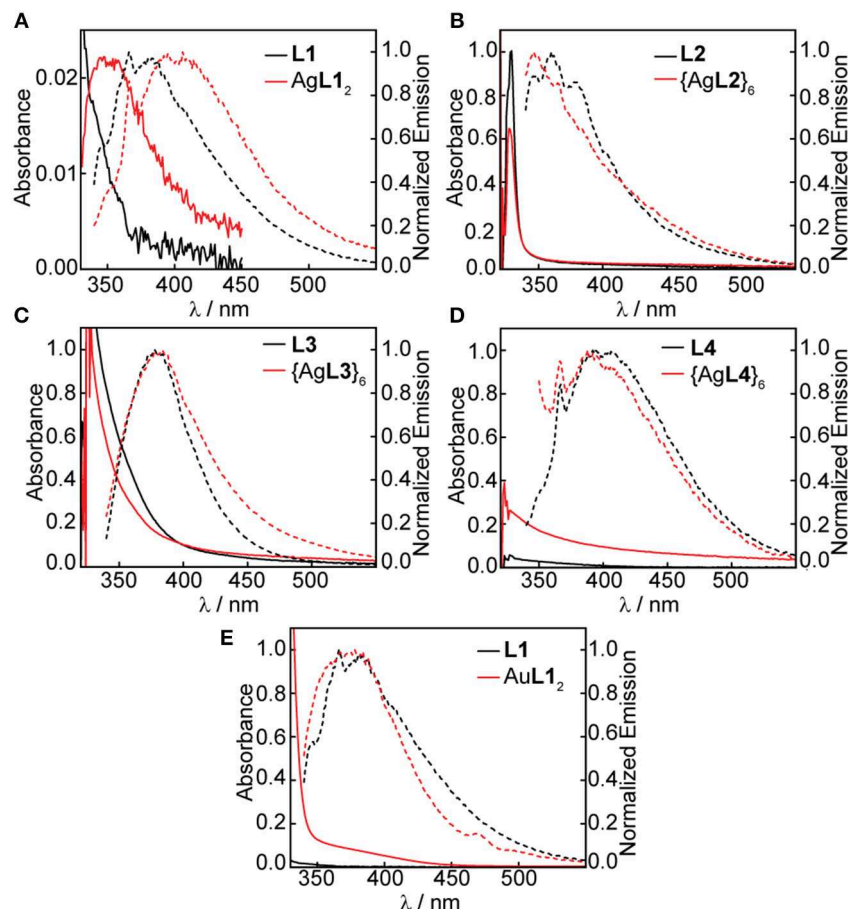


FIGURE 9 | UV-vis absorbance and emission spectra in acetone of (A) 0.10 mM L1 and saturated AgL1₂, (B) 0.10 mM L2 and saturated {AgL2}₆, (C) 0.10 mM L3 and saturated {AgL3}₆, and (D) 1.0 mM L4 and saturated {AgL4}₆, (E) 0.10 mM L1 and 0.10 mM AuL1₂.

TABLE 1 | Solution- and solid-state quantum yields and lifetimes of ligands, Ag and Au complexes and hexagons.

Compound	$\Phi_{\text{solid-state}}$, %	$\Phi_{\text{solution-state}}$, %	^a τ , ns	k_r , s ⁻¹	k_{nr} , s ⁻¹
L1	0.480	3.82	0.11	3.54×10^8	8.91×10^9
L2	0.180	0.800	0.12	6.45×10^7	8.00×10^9
L3	1.190	7.76	0.49	1.59×10^8	1.89×10^9
L4	0.010	~0.01*	0.10**	$<1.00 \times 10^6$	$>1.00 \times 10^{10}$
AgL1 ₂	0.200	2.32	0.10**	$>2.32 \times 10^8$	$>9.77 \times 10^9$
{AgL2} ₆	0.340	0.300	0.10**	$>3.00 \times 10^7$	$>9.97 \times 10^9$
{AgL3} ₆	0.130	4.70	0.17	2.83×10^8	5.74×10^9
{AgL4} ₆	0.510	~0.01*	0.10**	$<1.00 \times 10^6$	$>1.00 \times 10^{10}$
AuL1 ₂	0.06	1.12	0.11	1.04×10^8	9.19×10^9
{AuL2} ₆	0.170	***	***	***	***
{AuL3} ₆	0.010	***	***	***	***
{AuL4} ₆	0.110	***	***	***	***

^asolution-state quantum yield all measured in acetone.

*measured QY is below the instrumental limit of detection of 0.01%.

**measured lifetime is below the instrumental limit of detection of 0.10 ns.

***QY not measured due to instability in acetone.

non-radiative pathways are attenuated when intramolecular motions are reduced.

CONCLUSION

Silver(I) and gold(I) mononuclear complexes and hexagonal rings were self-assembled from AgPF₆ and Au(tht)Cl precursors and mono- and bidentate pyridyl ligands. These coordination resulting in self-assembly and complex formation was evidenced by the downfield ¹H NMR peak shifts of the ligand pyridyl H peaks and FT-ICR MS peaks with isotopic distributions and mass-to-charge ratios consistent with intact [6 + 6] cores that ionized by the loss of counterions.

Longer-term photostability of all complexes and hexagons in the solid-state were confirmed by FT-IR. Significant peak shifts to higher wavenumbers were observed upon coordination of the ligands to either Ag(I) or Au(I). No changes to the spectra were observed after storing the compounds at ambient conditions under room light for one week.

Ligand-centered fluorescence emission was observed for many of these complexes. In both the solid- and solution-state, **L3** and **L4** were the most and least emissive ligands, respectively. In the solid-state, all complexes and hexagons have diminished emission except for $\{\text{AgL2}\}_6$, $\{\text{AgL4}\}_6$, and $\{\text{AuL4}\}_6$ wherein aggregation-induced emission was observed. In the solution-state, all ligands and hexagons exhibited ligand-centered singlet emissions while AgL1_2 and AuL1_2 both exhibited metal-perturbed ligand-centered singlet emissions.

This work establishes that Ag(I) and Au(I) centers are effective linear nodes for self-assembly reactions with dipyrindyl ligands and that the resultant materials stabilize these ions with respect to oxidation and photodecomposition. Due to the modular nature of coordination-driven self-assembly, efforts are ongoing to exploit ligand-tuning to incorporate functional groups that will enhance metallacycle solubility to improve their processability for incorporation into mixed-matrix materials.

DATA AVAILABILITY

The dataset AgL1_2 (CCDC No. 1879931) for this study can be found in the Cambridge Crystallographic Data Centre <https://www.ccdc.cam.ac.uk/solutions/csd-system/components/csd/>.

REFERENCES

- Amayuelas, E., Fidalgo-Marijuan, A., Bazan, B., Urriaga, M. K., Barandika, G., and Arriortua, M.-I. (2016). CuII-based metal-organic nanoballs for very rapid adsorption of dyes and iodine. *Cryst. Eng. Comm.* 18, 1709–1712. doi: 10.1039/C5CE02511G
- Brown, C. J., Bergman, R. G., and Raymond, K. N. (2009). Enantioselective catalysis of the aza-cope rearrangement by a chiral supramolecular assembly. *J. Am. Chem. Soc.* 131, 17530–17531. doi: 10.1021/ja906386w
- Cao, A., Zhu, W., Shang, J., Klootwijk, J. H., Sudhölter, E. J. R., Huskens, J., et al. (2017). Metal-organic polyhedra-coated Si nanowires for the sensitive detection of trace explosives. *Nano Lett.* 17, 1–7. doi: 10.1021/acs.nanolett.6b02360
- Casini, A., Woods, B., and Wenzel, M. (2017). The promise of self-assembled 3D supramolecular coordination complexes for biomedical applications. *Inorg. Chem.* 56, 14715–14729. doi: 10.1021/acs.inorgchem.7b02599
- Chen, Q., Jiang, F., Yuan, D., Chen, L., Lyu, G., and Hong, M. (2013). Anion-driven self-assembly: from discrete cages to infinite polycatenanes step by step. *Chem. Commun.* 49, 719–721. doi: 10.1039/C2CC36921D
- Chen, X.-D., and Mak, T. C. W. (2005). Order of the coordinating ability of polyatomic monoanions established from their interaction with a disilver(i) metallacyclophane skeleton. *Chem. Commun.* 3529–3531. doi: 10.1039/B505919D
- Chevrier, I., Sagué, J. L., Brunetto, P. S., Khanna, N., Rajacic, Z., and Fromm, K. M. (2013). Rings, chains and helices: new antimicrobial silver coordination compounds with (iso-)nicotinic acid derivatives. *Dalton Trans.* 42, 217–231. doi: 10.1039/C2DT31259J
- Chia, Y. Y., and Tay, M. G. (2014). An insight into fluorescent transition metal complexes. *Dalton Trans.* 43, 13159–13168. doi: 10.1039/C4DT01098A
- Cook, T. R., and Stang, P. J. (2015). Recent developments in the preparation and chemistry of metallacycles and metallacages via coordination. *Chem. Rev.* 115:7001–45. doi: 10.1021/cr5005666
- Cook, T. R., Vajpayee, V., Lee, M. H., Stang, P. J., and Chi, K.-W. (2013). Biomedical and biochemical applications of self-assembled metallacycles and metallacages. *Acc. Chem. Res.* 46, 2464–2474. doi: 10.1021/ar400010v

AUTHOR CONTRIBUTIONS

CF designed and carried out the experiments and wrote the manuscript. SK assisted in ligand synthesis. AF carried out the mass spec characterization. TC designed the project and wrote the manuscript.

FUNDING

The project described was supported by Award Number S10RR029517 from the National Center For Research Resources.

ACKNOWLEDGMENTS

TC thanks the University at Buffalo for startup support resources. This work was completed using the resources of the Chemistry Instrument Center (CIC), University at Buffalo, SUNY, Buffalo, NY.

SUPPLEMENTARY MATERIAL

The Supplementary Material for this article can be found online at: <https://www.frontiersin.org/articles/10.3389/fchem.2019.00567/full#supplementary-material>

- Dechnik, J., Gascon, J., Doonan, C. J., Janiak, C., and Sumbly, C. J. (2017). Mixed-matrix membranes. *Angew. Chem. Int. Ed.* 56, 9292–9310. doi: 10.1002/anie.201701109
- Del Piero, S., Fedele, R., Melchior, A., Portanova, R., Tolazzi, M., and Zangrando, E. (2008). Solvation effects on the stability of silver(I) complexes with pyridine-containing ligands studied by thermodynamics and DFT methods. *Inorg. Chem.* 47, 1406–1406. doi: 10.1021/ic800010g
- Eldridge, R. B. (1993). Olefin/paraffin separation technology: a review. *Ind. Eng. Chem. Res.* 32, 2208–2212. doi: 10.1021/ie00022a002
- Fan, W.-J., Sun, B., Ma, J., Li, X., Tan, H., and Xu, L. (2015). Coordination-driven self-assembly of carbazole-based metallo dendrimers with generation-dependent aggregation-induced emission behavior. *Chem. Eur. J.* 21, 12947–12959. doi: 10.1002/chem.201501282
- Fernández, E. J., Laguna, A., López-de-Luzuriaga, J. M., Monge, M., Montiel, M., Olmos, M. E., et al. (2007). Pyridine gold complexes. an emerging class of luminescent materials. *Gold Bull.* 40, 172–183. doi: 10.1007/bf03215578
- Fox, B. S., Beyer, M. K., and Bondybey, V. E. (2002). Coordination chemistry of silver cations. *J. Am. Chem. Soc.* 124, 13613–13623. doi: 10.1021/ja0176604
- Fromm, K. M., Doimeadios, J. L. S., and Robin, A. Y. (2005). Concomitant crystallization of two polymorphs—a ring and a helix: concentration effect on supramolecular isomerism. *Chem. Commun.* 2005, 4548–4550. doi: 10.1039/B506389B
- Fujita, M. (1998). Metal-directed self-assembly of two- and three-dimensional synthetic receptors. *Chem. Soc. Rev.* 27, 417–425. doi: 10.1039/A827417Z
- Fujita, M., Umemoto, K., Yoshizawa, M., Fujita, N., Kusukawa, T., and Biradha, K. (2001). Molecular paneling coordination. *Chem. Commun.* 509–518. doi: 10.1039/B008684N
- Fulong, C. R. P., Liu, J., Pastore, V. J., Lin, H., and Cook, T. R. (2018). Mixed-matrix materials using metal-organic polyhedra with enhanced compatibility for membrane gas separation. *Dalton Trans.* 47, 7905–7915. doi: 10.1039/C8DT00082D
- Gimeno, M. C. (2009). “The chemistry of gold,” in *Modern Supramolecular Gold Chemistry*, ed A. Laguna (Wiley-VCH Verlag GmbH & Co. KGaA), 10–14. doi: 10.1002/9783527623778.ch1
- Huang, C.-B., Xu, L., Zhu, J.-L., Wang, Y.-X., Sun, B., Li, X., et al. (2017). Real-time monitoring the dynamics of coordination-driven self-assembly by

- fluorescence-resonance energy transfer. *J. Am. Chem. Soc.* 139, 9459–9462. doi: 10.1021/jacs.7b04659
- Ito, H., Kusakawa, T., and Fujita, M. (2000). Wacker oxidation in an aqueous phase through the reverse phase-transfer catalysis of a self-assembled nanocage. *Chem. Lett.* 29, 598–599. doi: 10.1246/cl.2000.598
- Jenkins, D. E., and Assefa, Z. (2017). Structural, photoluminescence, and theoretical DFT studies of gold(I) and silver(I) metallacycle dinuclear complexes of 1-methylbenzimidazolidenyl phosphine (MBDP) ligand. *J. Mol. Struct.* 1133, 374–383. doi: 10.1016/j.molstruc.2016.11.070
- Katritzky, A. R., and Hands, A. R. (1958). 448. Infrared studies of heterocyclic compounds. Part II. 2-Monosubstituted pyridines. *J. Chem. Soc.* 1958, 2202–2204. doi: 10.1039/JR9580002202
- Kim, C. W., Kim, C.-R., Noh, T. H., and Jung, O.-S. (2009). Ring-conformations via the competition of electrostatic interaction and argentophilic interaction. cyclodimeric structures of silver trifluoromethanesulfonate containing isonicotinate ester Ligands. *Bull. Kor. Chem. Soc.* 30:2341. doi: 10.5012/BKCS.2009.30.10.2341
- Kim, D.-S., and Ahn, K. H. (2008). Fluorescence “Turn-On” sensing of carboxylate anions with oligothiophene-based o-(Carboxamido)trifluoroacetophenones. *J. Org. Chem.* 73, 6831–6834. doi: 10.1021/jo801178y
- Kole, G. K., Tan, G. K., and Vittal, J. J. (2012). Photoreactivity of Ag(I) complexes and coordination polymers of pyridyl acrylic acids. *Crystal Growth Des.* 12, 326–332. doi: 10.1021/cg201119c
- Kuijpers, P. F., Otte, M., Dürr, M., Ivanović-Burmazović, I., Reek, J. N. H., and de Bruin, B. (2016). A self-assembled molecular cage for substrate-selective epoxidation reactions in aqueous media. *ACS Catal.* 6, 3106–3112. doi: 10.1021/acscatal.6b00283.
- Langdon-Jones, E. E., and Pope, S. J. A. (2014). Recent developments in gold(i) coordination chemistry: luminescence properties and bioimaging opportunities. *Chem. Commun.* 50, 10343–10354. doi: 10.1039/C4CC03259D
- Laye, R. H. (2007). Syntheses and photophysical properties of a series of [2:2] silver(I) metallacycles. *Inorg. Chim. Acta.* 360, 439–447. doi: 10.1016/j.ica.2006.07.068
- Leininger, S., Olenyuk, B., and Stang, P. J. (2000). Self-assembly of discrete cyclic nanostructures mediated by transition metals. *Chem. Rev.* 100, 853–908. doi: 10.1021/cr9601324
- Lin, J. C. Y., Tang, S. S., Vasam, C. S., You, W. C., Ho, T. W., Huang, C. H., et al. (2008). Structural, photophysical, and catalytic properties of Au(I) complexes with 4-substituted pyridines. *Inorg. Chem.* 47, 2543–2551. doi: 10.1021/ic701872f
- Mandal, A., Singha, M., Addy, P. S., and Basak, A. (2019). Laser desorption ionization mass spectrometry: Recent progress in matrix-free and label-assisted techniques. *Mass Spectrometry Rev.* 38, 3–21. doi: 10.1002/mas.21545
- Marin, M. L., McGilvray, K. L., and Scaiano, J. C. (2008). Photochemical strategies for the synthesis of gold nanoparticles from Au(III) and Au(I) using photoinduced free radical generation. *J. Am. Chem. Soc.* 130, 16572–16584. doi: 10.1021/ja803490n
- Mei, H.-X., Zhang, T., Wang, D.-F., Huang, R.-B., and Zheng, L.-S. (2015a). Metallacycles or coexistence of isomeric metallacycle and chain: Anion-dependent luminescent Ag complexes of a flexible diaminotriazine–imidazole ligand. *J. Mol. Struct.* 1091, 57–64. doi: 10.1016/j.molstruc.2015.02.030
- Mei, J., Leung, N. L. C., Kwok, R. T. K., Lam, J. W. Y., and Tang, B. Z. (2015b). Aggregation-induced emission: together we shine, united we soar! *Chem. Rev.* 115, 11718–11940. doi: 10.1021/acs.chemrev.5b00263
- Ren, Y. P., Kong, X.-J., Long, L.-S., Huang, R.-B., and Zheng, L.-S. (2006). Anion-dependent assembly of cyclic structure. *Crystal Growth Des.* 6, 572–576. doi: 10.1021/cg050459a
- Riddell, I. A., Smulders, M. M. J., Clegg, J. K., and Nitschke, J. R. (2011). Encapsulation, storage and controlled release of sulfur hexafluoride from a metal–organic capsule. *Chem. Commun.* 47, 457–459. doi: 10.1039/C0CC02573A
- Schrader, B. (2007). “Infrared and Raman spectroscopy: methods and applications,” in *Infrared and Raman Spectroscopy*, ed B. Schrader (Wiley-VCH Verlag GmbH), 711–764. doi: 10.1002/9783527615438.refs
- Shakirova, J. R., Tomashenko, O. A., Grachova, E. V., Starova, G. L., Sizov, V. V., Khelebnikov, A. F., et al. (2017). Gold(I)–alkynyl complexes with an N-donor heterocyclic ligand: synthesis and photophysical properties. *Eur. J. Inorg. Chem.* 2017, 4180–4186. doi: 10.1002/ejic.201700731
- Shin, D. M., Lee, I. S., Lee, Y.-A., and Chung, Y. K. (2003). Self-assembly between silver(I) and Di- and Tri-2-pyridines with flexible spacer: formation of discrete metallacycle versus coordination polymer. *Inorg. Chem.* 42, 2977–2982. doi: 10.1021/ic0260163
- Smulders, M. M. J., and Nitschke, J. R. (2012). Supramolecular control over Diels–Alder reactivity by encapsulation and competitive displacement. *Chem. Sci.* 3, 785–788. doi: 10.1039/C1SC00847A
- Sudik, A. C., Millward, A. R., Ockwig, N. W., Côté, A. P., Kim, J., and Yaghi, O. M. (2005). Design, synthesis, structure, and gas (N₂, Ar, CO₂, CH₄, and H₂) sorption properties of porous metal–organic tetrahedral and heterocuboidal polyhedra. *J. Am. Chem. Soc.* 127, 7110–7118. doi: 10.1021/ja042802q
- Tang, J.-H., Sun, Y., Gong, Z.-L., Li, Z.-Y., Zhou, Z., Wang, H., et al. (2018). Temperature-responsive fluorescent organoplatinum(II) metallacycles. *J. Am. Chem. Soc.* 140, 7723–7729. doi: 10.1021/jacs.8b04452
- Tashiro, S., Tominaga, M., Kawano, M., Therrien, B., Ozeki, T., and Fujita, M. (2005). Sequence-selective recognition of peptides within the single binding pocket of a self-assembled coordination cage. *J. Am. Chem. Soc.* 127, 4546–4547. doi: 10.1021/ja044782y
- Vardhan, H., and Verpoort, F. (2015). Metal–organic polyhedra: catalysis and reactive intermediates. *Adv. Synt. Catal.* 357, 1351–1368. doi: 10.1002/adsc.201400778
- Vikse, K. L., and Scott McIndoe, J. (2018). Ionization methods for the mass spectrometry of organometallic compounds. *J. Mass Spectromet.* 53, 1026–1034. doi: 10.1002/jms.4286
- Wan, C.-Q., and Mak, T. C. W. (2011). Unusual carbonyl...carbonyl interaction in supramolecular structures of silver(I) complexes with 2,6-Pyridinediylbis(4-pyridinyl)methanone. *Crystal Growth Des.* 11, 832–842. doi: 10.1021/cg101490a
- Wang, J., He, C., Wu, P., Wang, J., and Duan, C. (2011). An amide-containing metal–organic tetrahedron responding to a spin-trapping reaction in a fluorescent enhancement manner for biological imaging of NO in living cells. *J. Am. Chem. Soc.* 133, 12402–12405. doi: 10.1021/ja2048489
- Wei, W., Yu, H., Jiang, F., Liu, B., Ma, J., and Hong, M. (2012). Anion-controlled conformational variation: structural modulation and anion exchange of Ag(i) coordination networks. *Cryst. Eng. Comm.* 14, 1693–1700. doi: 10.1039/C1CE06141K
- Yang, H.-B., Ghosh, K., Northrop, B. H., Zheng, Y.-R., Lyndon, M. M., Muddiman, D. C., et al. (2007). A highly efficient approach to the self-assembly of hexagonal cavity-cored Tris[2]pseudorotaxanes from several components via multiple noncovalent interactions. *J. Am. Chem. Soc.* 129, 14187–14189. doi: 10.1021/ja073744m
- Yeşilel, O. Z., Karamahmut, B., Semerci, F., and Yeşilöz, Y. (2012). Synthesis, crystal structures, spectroscopic and thermal properties of silver(I) saccharinate complexes with N-donor ligands. *Polyhedron* 42, 307–314. doi: 10.1016/j.poly.2012.05.034
- Zhao, D., Yuan, D., Krishna, R., van Baten, J. M., and Zhou, H.-C. (2010). Thermosensitive gating effect and selective gas adsorption in a porous coordination nanocage. *Chem. Commun.* 46, 7352–7354. doi: 10.1039/C0CC02771E
- Zhou, J., Liu, X., Zhang, Y., Li, B., and Zhang, Y. (2006). Synthesis, structures and luminescent properties of two silver supramolecular isomers with one-dimensional concavo-convex chain and dimer metallacycle. *Inorg. Chem. Commun.* 9, 216–219. doi: 10.1016/j.inoche.2005.11.001
- Zwijnenburg, M. A., Berardo, E., Peveler, W. J., and Jelfs, K. E. (2016). Amine molecular cages as supramolecular fluorescent explosive sensors: a computational perspective. *J. Phys. Chem. B* 120, 5063–5072. doi: 10.1021/acs.jpcc.6b03059

Conflict of Interest Statement: The authors declare that the research was conducted in the absence of any commercial or financial relationships that could be construed as a potential conflict of interest.

Copyright © 2019 Fulong, Kim, Friedman and Cook. This is an open-access article distributed under the terms of the Creative Commons Attribution License (CC BY). The use, distribution or reproduction in other forums is permitted, provided the original author(s) and the copyright owner(s) are credited and that the original publication in this journal is cited, in accordance with accepted academic practice. No use, distribution or reproduction is permitted which does not comply with these terms.